Electronic Structure Description of a Doubly Oxidized Bimetallic Cobalt Complex with Pro-Radical Ligands

Ryan M. Clarke,[†] Khatera Hazin,[†] John R. Thompson,[†] Didier Savard,[†] Kathleen E. Prosser,[†] and Tim Storr*[,†]

[†]Department of Chemistry, Simon Fraser University, Burnaby, British Columbia, V5A 1S6, Canada

Bimetallic complexes; cobalt; ligand radical; delocalization; electronic structure

ABSTRACT: The geometric and electronic structure of a doubly oxidized bimetallic Co complex containing two redox-active salen moieties connected *via* a 1,2-phenylene linker has been investigated and compared to an oxidized monomeric analogue. Both complexes, **CoL^1** and **Co$_2$L^2** are oxidized to the mono- and di-cations respectively with $AgSbF_6$ and characterized by X-ray crystallography for the monomer, and Vis-NIR spectroscopy, electron paramagnetic (EPR) spectroscopy, SQUID magnetometry and density functional theory (DFT) calculations for both the monomer and dimer. Both complexes exhibit a water molecule coordinated in the apical position upon oxidation. **[CoL^1-H$_2$O]$^+$** displays a broad NIR band at 8500 cm^{-1} (8400 M^{-1}cm^{-1}) which is consistent with recent reports on oxidized Co salen complexes (Kochem, A. et. al., *Inorg Chem.*, **2012**, *51*, 10557-10571, Kurahashi, T. et. al., *Inorg. Chem.*, **2013**, *52*, 3908-3919). DFT calculations predict a triplet ground state with significant ligand *and* metal contributions to the singularly occupied molecular orbital (SOMO). The majority (~75%) of the total spin density is localized on the metal, highlighting both high spin Co(III) and Co(II)L• character in the electronic ground state. Further oxidation of CoL^1 to the dication affords a low spin Co(III) phenoxyl radical species. The NIR features for **[Co$_2$L^2-2H$_2$O]$^{2+}$** at 8600 cm^{-1} (17800 M^{-1}cm^{-1}) are doubly intense in comparison to **[CoL^1-H$_2$O]$^+$** owing to the description of **[Co$_2$L^2-2H$_2$O]$^{2+}$** as two non-interacting oxidized Co salen complexes bound *via* the central phenylene linker. Interestingly, TD-DFT calculations predict two electronic transitions that are 353 cm^{-1} apart. The NIR spectrum of the analogous Ni complex, [**Ni$_2$L^2]$^{2+}$**, exhibits two intense transitions (4890 cm^{-1}/26500 M^{-1}cm^{-1} and 4200 cm^{-1}/21200 M^{-1}cm^{-1}) due to exciton coupling in the excited state. Only one broad band is observed in the NIR spectrum for **[Co$_2$L^2-2H$_2$O]$^{2+}$** as a result of the contracted donor and acceptor orbitals and overall CT character.

1. Introduction

The relationship between electronic structure and reactivity in inorganic complexes is an area of considerable research interest; with the interplay between metal ions and redox-active ligands receiving particular attention.[1] Many metalloenzymes couple one electron redox changes at metal centers with redox-active ligands in order to promote multielectron chemistry.[2] Classic examples include galactose oxidase[3] and cytochrome p450,[4] two enzymes with first row transition metal centers coupled to pro-radical ligands in order to drive substrate turnover. Owing to the simplicity of the active sites, many structural and functional small-molecule models of these and other enzymes have been studied.[5]

Depending on the relative energy of redox-active orbitals, metal complexes with proradical ligands ([M^{n+}L]) can undergo ligand-based ([M^{n+}L•]$^+$) or metal-based ([M($^{n+1}$)L]$^+$) oxidation. Classes of redox-active ligands include dithiolenes,[6] dioxolenes,[7] diimines,[8] and phenol containing ligands.[9] One class of redox-active ligand that has been studied extensively are tetradentate salen ligands (salen is a common abbreviation for N_2O_2 bis-Schiff-base bis-phenolate ligands), due to their facile and modular syntheses and highly tunable steric and electronic properties.[5g, 10] Monometallic salen complexes have been studied in applications ranging from catalysis[11] to self-assembly.[12] Interestingly, numerous reactivity studies involving metal-salen complexes have demonstrated second-order kinetic dependence with respect to the metallosalen catalyst.[13] As a result, multiple catalytic sites have been incorporated into the same molecule as a means to enhance reactivity, and oftentimes cooperativity was observed.[14] The performance of multimetallic salen catalysts is however greatly dependent on factors such as the distance and orientation between the catalytic sites as well as the nature of the linker group employed.[13, 15] Further interest in multimetallic salen complexes arises from their interesting electronic structure,[16] magnetism[17] and supramolecular properties.[18]

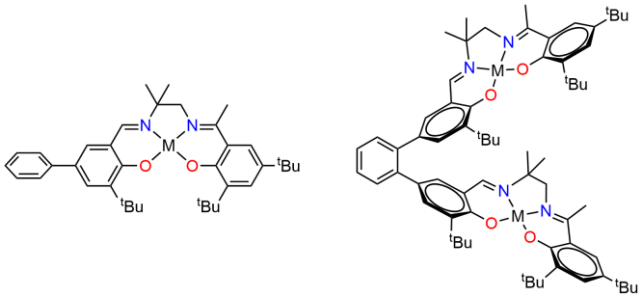

Chart 1. Monometallic and bimetallic salen complexes studied. M = Ni, previous work.[16a] M = Co, this work.

Although studied extensively in the context of catalysis, the ligand radical chemistry of multimetallic salen complexes has received comparatively little attention.[16b, 16c, 19] We have previously studied the geometric and electronic structures of a monometallic Ni salen complex and its bimetallic analogue (Chart 1).[16a] Upon oxidation with a suitable chemical oxidant, the

bimetallic Ni salen complex can be oxidized to a bis-ligand radical species. Herein, we extend this work to Co complexes as a means to study the interplay between redox active salen ligands and more easily oxidizable metal centers. The structure of the bimetallic Co complex bears resemblance to the co-facial Co porphyrins studied by Collman *et. al.*,[20] Nocera *et. al.*,[21] and Co calixpyrroles studied by Love and co-workers.[22] Co complexes involving redox active ligands, and in particular Co(II)-bis(phenolate) complexes have been investigated due to the interesting electronic structures of both neutral and oxidized species. Examples include work by Benisvy *et al.* in which a Co(II) complex involving two imidazole-phenolate ligands undergoes one electron oxidation to afford a complex bearing one phenoxyl radical and a phenolate moiety bound to a Co(II) center, rather than a Co(III)-bis(phenolate) complex.[23] Interestingly, both tetracoordinated Co(II) and square pyramidal Co(III) complexes with radical *o*-iminobenzosemiquinonate type ligands have also been reported.[24] Additionally, benzenedithiolate and *o*-phenylenediamine ligands have been shown to afford Co complexes with dithiosemiquinato and *o*-diiminobenzosemiquinato radicals upon oxidation.[25] Co salen complexes have been studied extensively for their use in a number of catalytic reactions including kinetic hydrolytic resolution of epoxides[26] and the nitro-aldol reaction.[14c]. Furthermore, the electronic structures of their oxidized forms have been shown to be sensitive to factors such as exogenous ligands, counter ions, and solid state packing effects.[27] In this work, through both extensive experimental and theoretical characterization techniques, we show that upon one and two electron oxidation, respectively, monometallic and bimetallic Co salen complexes form species with ligand radical character. However, significant metal contribution to the singularly occupied molecular orbital results in a less delocalized electronic structure in comparison to the Ni analogues, resulting in a much broader low energy absorption band in the Vis-NIR spectrum lacking observable splitting due to exciton coupling.

2. Experimental

2.1. Materials and Methods. All chemicals used were of the highest grade available and were further purified whenever necessary.[28] The ligands, 1-(2-hydroxy-3,5-di-tert-butylphenyl)-methyl-2,5-diimine-4,4-dimethyl-6-(2-hydroxy-3-tert-butyl-5-phenyl) phenyl, (H_2L^1) and (1,2-Bis-(1-(2-hydroxy-3,5-di-tert-butylphenyl)-methyl-2,5-diimine-4,4-dimethyl-6-(2-hydroxy-3,5-di-tert-butylphenyl)-benzene, (H_4L^2) were synthesized according to published procedures.[16a] The aminium radical chemical oxidant $[N(C_6H_3Br_2)_3]^{+\bullet}[SbF_6]^-$ was synthesized according to published protocols.[29] Electronic spectra were recorded on a Cary 5000 spectrophotometer with a custom-designed immersion fiber-optic probe with variable path-length (1 and 10 mm; Hellma, Inc.). Constant temperatures were maintained by a dry ice/acetone bath. Solvent contraction was accounted for in all variable temperature studies. Cyclic voltammetry (CV) was performed on a PAR-263A potentiometer, equipped with an Ag wire reference electrode, a Pt disk working electrode, and a Pt counter electrode with nBu_4NClO_4 (0.1 M) solution in CH_2Cl_2. Decamethylferrocene was used as an internal standard. ^{1}H NMR spectra were recorded on a Bruker AV-500 instrument. Solution paramagnetic susceptibilities were calculated using the Evans method.[30] Mass spectra (positive ion) were obtained on a Bruker Microflex LT MALDI-TOF MS instrument. Elemental analyses (C, H, N) were performed by Mr. Farzad Haftbaradaran and Mr. Paul Mulyk at Simon Fraser University on a Carlo Erba EA1110 CHN elemental analyser. Electron paramagnetic resonance (EPR) spectra were collected using a Bruker EMXplus spectrometer operating with a premiumX X-band microwave bridge and an HS resonator. Low temperature measurements of frozen solutions used a Bruker ER 4112HV helium temperature-control system and continuous flow cryostat. Samples for X-band EPR measurements were placed in 4 mm outer-diameter sample tubes with sample volumes of approximately 500 μL.

2.2. Synthesis. *2.2.1. Synthesis of* ***CoL^1***. To a solution of ligand H_2L^1 (340 mg, 0.6 mmol) in diethyl ether (4 mL) was added a $Co(OAc)_2$•$4H_2O$ solution (155 mg, 0.6 mmol in 4 mL methanol) under anaerobic conditions. The solution immediately turned from yellow to red upon addition and was stirred at room temperature until a dark red precipitate formed. The precipitate was collected and dried in vacuo. The dark red powder was recrystallized by slow diffusion of methanol into a concentrated CH_2Cl_2 solution of **CoL^1** to afford block-like red crystals. Yield: 290 mg, 74%. Elemental analysis: calculated for $C_{37}H_{48}CoN_2O_2$: C 72.65, H 7.91, N 4.58; found: C 72.97 H 7.63 N 4.64. MALDI-MS *m/z*: 611.30 (100%). Solution magnetic moment (^{1}H Evan's Method): μ_{eff} = 1.75.

2.2.2. Synthesis of ***[CoL^1-H$_2$O]$^+$***. To a solution of **CoL^1** (110 mg, 0.18 mmol) in CH_2Cl_2 (3 mL) was added a $AgSbF_6$ solution (60 mg, 0.18 mmol in 3 mL CH_2Cl_2) under anaerobic conditions. The solution immediately turned from red to dark green upon addition of oxidant and was stirred at room temperature for 30 minutes. The reaction mixture was filtered through Celite and concentrated in vacuo. The crude material was redissolved in dichlormethane (2 mL) and pentane was added (2 mL) to precipitate a dark green powder. Crystals suitable for X-ray analysis were grown by slow diffusion of pentane into a concentrated CH_2Cl_2 solution. Yield: 132 mg, 85%. Elemental analysis: calculated for $C_{37}H_{50}CoN_2O_3SbF_6$•$H_2O$. C 50.30, H 5.93, N 3.17; found: C 49.92, H 5.90, N 2.97. Solution magnetic moment (^{1}H Evan's Method) μ_{eff} = 2.62.

2.2.3. Synthesis of ***Co$_2$L^2***. To a solution of ligand H_4L^2 (400 mg, 0.4 mmol) in diethyl ether (5 mL) was added a $Co(OAc)_2$•$4H_2O$ solution (190 mg, 0.8 mmol in 5mL methanol) under anaerobic conditions. The solution immediately turned from yellow to red upon addition and was stirred at room temperature until a dark red precipitate formed. The precipitate was collected and dried in vacuo. The dark red powder was recrystallized by slow diffusion of methanol into a concentrated CH_2Cl_2 solution of **Co$_2$L^2** to afford block-like red crystals. Yield: 200 mg, 45%. MALDI-MS *m/z:* 1144.48 (100%). Elemental analysis: calculated for $C_{68}H_{90}Co_2N_4O_4$•CH_2Cl_2: C 67.36, H 7.54, N 4.55; found: C 67.25, H 7.61, N 4.27. Solution magnetic moment (^{1}H Evan's Method): μ_{eff} = 2.75.

2.2.4. Synthesis of ***[Co$_2$L^2-2H$_2$O]$^{2+}$***. To a solution of **Co$_2$L^2** (150 mg, 0.13 mmol) in CH_2Cl_2 (5 mL) was added a $AgSbF_6$ solution (90 mg, 0.26 mmol in 5 mL CH_2Cl_2) under anaerobic conditions. The solution immediately turned from red to dark

green upon addition of oxidant and was stirred at room temperature for 30 minutes. The reaction mixture was filtered through celite and concentrated in vacuo. The crude solid was redissolved in CH_2Cl_2 (2 mL) and pentane was added (2 mL) to afford a green precipitate. Yield: 168 mg, 70%. Elemental analysis: calculated for $C_{68}H_{94}Co_2N_4O_6Sb_2F_{12}$: C 49.41, H 5.73, N 3.39; found: C 49.12, H 5.47, N 3.40.

2.3. X-ray Structure Determination. *CoL^1*. Single crystal X-ray crystallographic analysis of a block-red crystal of **CoL^1** was carried out at the Advanced Light Source (Lawrence Berkeley National Laboratory) using synchrotron radiation tuned to λ=0.7749 Å. Intensity data were collected at 296K on a D8 goniostat equipped with a Bruker APEXII CCD detector at Beamline 11.3.1. For data collection frames were measured for a duration of 1 s at 0.3° intervals of ω with a maximum 2θ value of ~60°. The data frames were collected using the program APEX2 and processed using the program SAINT routine within APEX2. The data were corrected for absorption and beam corrections based on the multi-scan technique as implemented in SADABS. The structure was solved by the intrinsic phasing method[31] and subsequent refinements were performed using ShelXle.[32] All non-hydrogen atoms were refined anisotropically. All C-H hydrogen atoms were placed in calculated positions by were not refined.

$[CoL^1\text{-}H_2O]^+$. Crystallographic analysis of **$[CoL^1\text{-}H_2O]^+$** was performed on a Bruker APEX II Duo diffractometer with graphite monochromated Cu-Kα radiation. A dark green block crystal was mounted on a 150 μm MiteGen sample holder. The data were collected at 293K to a maximum 2θ value of ~60°. Data were collected in a series of ϕ and ω in 0.50° widths with 10.0 s exposures. The crystal-to-detector distance was 50 mm. The structure was solved by intrinsic phasing[31] and refined by least-squares procedures using Crystals.[33] **$[CoL^1\text{-}H_2O]^+$** crystallizes with one molecule of CH_2Cl_2 solvent in the asymmetric unit. All non-hydrogen atoms were refined anisotropically. All C-H hydrogen atoms were placed in calculated positions but were not refined.

Co_2L^2. Crystallographic analysis of **Co_2L^2** was performed on a Bruker X8 APEX II diffractometer with graphite monochromated Mo-Kα radiation. An irregular red crystal was mounted on a glass fibre. The data were collected at a temperature of -103.15 ± 0.1 K to a maximum 2θ value of 45.0°. Data were collected in a series of ϕ and ω scans in 0.50° widths with 30.0 s exposures. The crystal-to-detector distance was 40 mm. The complex crystallizes as a two-component twin with the two components related by a 180° rotation about the (0 -0.5 1) reciprocal axis. Data were integrated for both twin components, including both overlapped and non-overlapped reflections. The structure was solved by direct methods using non-overlapped data from the major twin component. Subsequent refinements were carried out using an HKLF5 format data set containing complete data from component 1 and any overlapped reflections from component 2. The material crystallizes with two **Co_2L^2** complexes and hexane solvent in the asymmetric unit. The solvent molecules are disordered and cannot be modeled properly, thus the PLATON/SQUEEZE[34] program was used to generate a 'solvent-free' HKLF5 format data set. The equivalent of 4 molecules of hexane were removed from the asymmetric unit. All non-hydrogen atoms were refined anisotropically. All hydrogen atoms were included in calculated positions but were not refined. The batch scale refinement showed a roughly 57:43 ratio between major and minor twin components. All crystal structure plots were produced using ORTEP-3[35] and rendered with POV-Ray (v.3.6.2).[36] A summary of the crystal data and experimental parameters for structure determinations is given in Table S1.

2.4. Calculations. Geometry optimizations were performed using the Gaussian 09 program (Revision D.01),[37] the B3LYP functional,[38] and the 6-31G(d) basis set on all atoms as this functional/basis set combination has afforded a good match to experimental metrical data in similar salen systems.[16a-c] Frequency calculations at the same level of theory confirmed that the optimized structures were located at a minimum on the potential energy surface. Single point calculations for energetic analysis were performed with the B3LYP functional and the TZVP basis set of Ahlrichs on all atoms.[39] Broken-symmetry (BS) density functional theory (DFT) calculations were performed with the same functional and basis set.[40] The intensities of the 30 lowest energy electronic transitions were calculated by TD-DFT[41] at the B3LYP/TZVP level with a polarized continuum model (PCM) for CH_2Cl_2.[42] AOMix was used for determining atomic orbital compositions employing Mulliken population analysis.[43]

2.5. Solid State Magnetism. The magnetic properties of **Co_2L^2**, **$[CoL^1\text{-}H_2O]^+$**, and **$[Co_2L^2\text{-}2H_2O]^{2+}$** were measured using a Quantum Design MPMS-XL7 SQUID magnetometer operating between 1.8 and 300 K for dc applied fields ranging between -7 and 7 T. The measurements were performed on polycrystalline samples of 16.2, 23.7 and 20.4 mg, for **Co_2L^2**, **$[CoL^1\text{-}H_2O]^+$**, and **$[Co_2L^2\text{-}2H_2O]^{2+}$** respectively, wrapped in a polyethylene membrane. The data was corrected for the diamagnetic contribution of the sample holder and of the complexes.

3. Results

3.1. Synthesis and Characterization of Neutral Complexes. CoL^1 and **Co_2L^2** (Chart 1) were prepared by treating diethyl ether solutions of the corresponding ligand (H_2L^1 or H_4L^2) with methanolic solutions of $Co(OAc)_2 \cdot 4H_2O$ under anaerobic conditions. Recrystallization of **CoL^1** and **Co_2L^2** afforded crystals suitable for X-ray analysis in moderate yields. Solution magnetic susceptibility measurements (^{1}H NMR Evan's Method) revealed the presence of a low spin, $S = ½$ d^7 Co(II) ground state for **CoL^1** ($\mu_{eff} = 1.75$) and an $S = 1$ ground state for **Co_2L^2** ($\mu_{eff} = 2.75$), originating from two independent $S = ½$ d^7 Co(II) centers (*vide infra*). Both compounds display paramagnetically shifted ^{1}H NMR spectra. For **CoL^1** (Figure S1), two sets of resonances are discernible in certain regions of the spectra, originating from the asymmetric salen construct.[27b] The ^{1}H NMR spectrum for **Co_2L^2** (Figure S1) is similar to **CoL^1**, however the compound displayed lower solubility. The solid-state structure of **Co_2L^2** is presented in Figure 1, while the solid-state structure of **CoL^1** is presented in the Supporting

Information (Figure S2). Select crystallographic data are shown in Table S1. **Co_2L^2** crystalizes with two molecules of **Co_2L^2** in the asymmetric unit (Figure S3). Each molecule has two Co(II) ions; each in a distorted square planar geometry bound via the expected N_2O_2 coordination sphere of the salen moieties. The average intramolecular metal-metal distance is 10 Å. Furthermore, the bimetallic complex exists in a *cis* conformation in the solid state, in which the bulky *tert*-butyl substituents are aligned on the same side of the molecule, similar to the analogous Ni complex.[16a] The structure of **Co_2L^2** in solution was investigated further by variable temperature ^{1}H NMR spectroscopy (Figure S4). While not as definitive as the data for the Ni complex due to paramagnetic signal broadening, splitting of the resonance at -11 ppm and increased signal broadening in the aromatic region suggests rotational restriction of the salen units at low temperature.

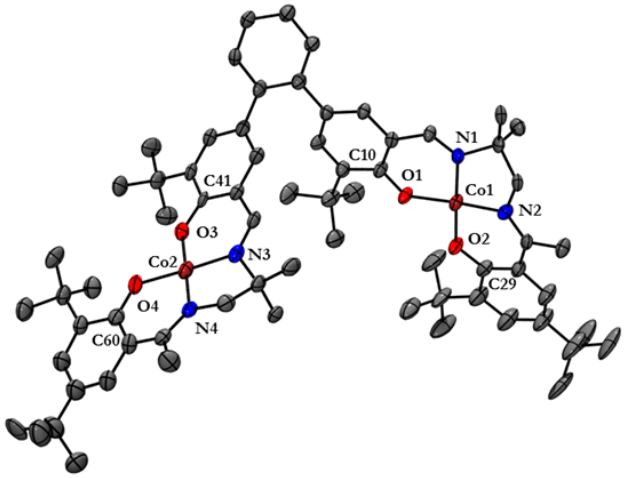

Figure 1. ORTEP plot of **Co_2L^2** (50% probability) using POV-Ray, excluding hydrogen atoms and solvent. Selected interatomic distances [Å] and angles [°]: Co(1)-O(1): 1.874, Co(1)-O(2): 1.830, Co(1)-N(1): 1.841, Co(1)-N(2): 1.870, C(10)-O(1): 1.317, C(29)-O(2): 1.321, Co(2)-O(3): 1.859, Co(2)-O(4): 1.840, Co(2)-N(3): 1.855, Co(2)-N(4): 1.894, C(41)-O(3): 1.329, C(60)-O(4): 1.310, Co(1)-Co(2): 10.04; angles: O(1)-Co(1)-N(1): 92.7, O(1)-Co(1)-O(2): 87.8, O(1)-Co(1)-N(2): 173.2, O(2)-Co(1)-N(2): 92.8, O(2)-Co(1)-N(1): 176.2, N(1)-Co(1)-N(2): 87.1, O(3)-Co(2)-N(3): 92.3, O(3)-Co(2)-O(4): 87.6, O(3)-Co(2)-N(4): 178.0, O(4)-Co(2)-N(4): 92.5, O(4)-Co(2)-N(3): 177.3, N(3)-Co(2)-N(4): 87.5.

3.2. Electrochemistry. Redox processes for **CoL^1** and **Co_2L^2** were probed by cyclic voltammetry (CV) in CH_2Cl_2 using tetra-*n*-butyl-ammonium perchlorate (nBu_4NClO_4) as the supporting electrolyte (Figure 2).The redox processes versus ferrocenium/ferrocene (F_c^+/F_c) are reported in Table 1. A quasi-reversible one-electron redox process is observed for **CoL^1** at 0.16 V *vs* F_c^+/F_c. An additional two-electron quasi-reversible redox process is observed at 0.76 V (see **3.8** for further discussion). The redox processes are similar to those reported by Thomas and co-workers for a symmetric tBu substituted Co salen complex (0.01 V and 0.7 V *vs* F_c^+/F_c), albeit shifted to slightly more positive potentials.[27a] The small change is likely due to slight differences in ligand electronics. Furthermore, Thomas and co-workers observe a third redox wave at 0.74 V, which nearly overlaps the second wave at 0.7 V. In our case, we could not further resolve the two-electron process at 0.76 V (assigned in comparison to the internal standard F_c^*). Fujii and co-workers have also investigated the electronic structure of a symmetric tBu substituted Co salen complex with an axially bound triflate.[27b] In this case, the first observed redox wave was at -0.101 V, 0.26 V more negative than observed for **CoL^1**. A number of factors may play a role in this more negative potential, including nBu_4OTf as the supporting electrolyte, as well as the use of preoxidized complex in their studies. **Co_2L^2** displays very similar oxidation processes in comparison to **CoL^1** (Figure 2), however, the current intensities are effectively double with a two-electron redox process observed at 0.14 V while a four-electron process is observed at 0.78 V. This data shows that the two Co salen units are effectively isolated, with no observable splitting of the redox waves at the limit of spectral resolution.

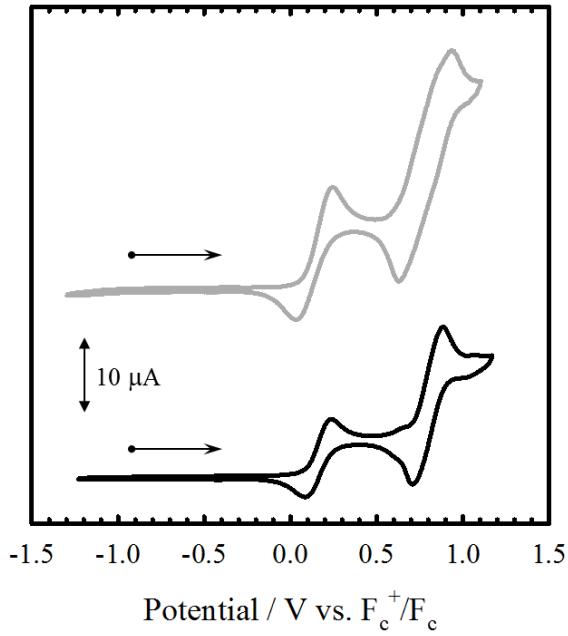

Figure 2. Cyclic voltammogram of **CoL^1** (black) and **Co_2L^2** (gray). Conditions: 2.5 mM complex, 0.1 M nBu_4NClO_4, scan rate 100 mV s^{-1}, CH_2Cl_2, 233 K.

Table 1. Redox Potentials of **CoL^1** and **Co_2L^2** versus F_c^+/F_c [a] given in V. Peak to peak separation given in parentheses

Compound	E_{pa}^1	E_{pc}^1	$E_{1/2}^1$	E_{pa}^2	E_{pc}^2	$E_{1/2}^2$
CoL^1	0.25	0.08	0.16 (0.17)	0.86	0.66	0.76 (0.20)
Co_2L^2	0.25	0.03	0.14 (0.23)	0.94	0.63	0.78 (0.30)

[a]Peak to peak difference for F_c^{*+}/F_c^* couple at 233K is 0.15V.

3.3. Synthesis and Characterization of Oxidized Complexes. Bulk oxidation of neutral complexes was carried

out under a dinitrogen atmosphere using $AgSbF_6$ as the oxidant (0.65 V *vs.* F_c^+/F_c in CH_2Cl_2).[44] **[CoL^1-H$_2$O][SbF$_6$]** was recrystallized from CH_2Cl_2/pentane solution and the molecular structure is presented in Figure 3, with select crystallographic data presented in Table S1. The solid state structure of **[CoL^1-H$_2$O]$^+$** exhibits a slightly distorted square pyramidal geometry with the expected N_2O_2 coordination sphere from the salen ligand as well as an apically bound water molecule. A close contact exists between a hydrogen of the axially bound water molecule and a F atom of the SbF_6 counterion (F4-O3 distance of 2.844 Å). The Co ion is displaced by 0.147 Å above the plane of the coordinating atoms of the salen ligands towards the O3 atom. Upon oxidation the Co-O bond lengths remain essentially the same in comparison to **CoL^1**, however the Co-N bonds become slightly elongated (Table 3). Similar structural data has been reported by Thomas *et al.* for a *para*-OMe substituted Co salen complex.[27a] The presence of paramagnetically shifted ^{1}H NMR signals is a strong indication that the electronic structure does not consist of a low spin Co(III) central metal ion. Furthermore, as shown in Figures S5 and S6, the paramagnetic effects are enhanced upon complex oxidation with the spectral window of **CoL^1** widening from -10 → 25 ppm to -35 → 60 ppm when oxidized. Similar shifting patterns are observed in the work by Fujii and co-workers which is attributable to ligand based radical contributions to the overall electronic structure.[27b, 45] We were unable to isolate X-ray quality crystals of **[Co$_2$L^2-2H$_2$O][SbF$_6$]$_2$**, although the compound was characterized by a number of analytical and spectroscopic methods. MS analysis of the oxidized complexes did not afford the expected molecular ions (ESI-MS or MALDI) due to loss of the apical water ligand.

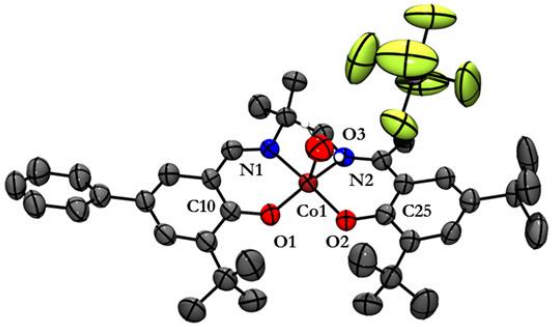

Figure 3. ORTEP plot of **[CoL^1-H$_2$0]$^+$** (50% probability) using POV-Ray, excluding hydrogen atoms and solvent. Selected interatomic distances [Å] and angles [°]: Co(1)-O(1): 1.868, Co(1)-O(2): 1.846, Co(1)-N(1): 1.891, Co(1)-N(2): 1.892, Co(1)-O(3): 2.124, C(10)-O(1): 1.324, C(25)-O(2): 1.326; angles: O(1)-Co(1)-N(1): 93.4, O(1)-Co(1)-O(2): 87.7, O(1)-Co(1)-N(2): 170.1, O(2)-Co(1)-N(2): 97.1, O(2)-Co(1)-N(1): 171.7, N(1)-Co(1)-N(2): 85.8, O(3)-Co(1)-O(1): 91.7, O(3)-Co(1)-N(1): 96.4, O(3)-Co(1)-O(2): 91.8, O(3)-Co(1)-N(2): 98.1.

3.4. Electronic Absorption Spectroscopy. The solution electronic absorption spectra of neutral and oxidized **CoL^1** and **Co$_2$L^2** in the Vis-NIR region are shown in Figure 4. Both neutral complexes are characterized by intense CT transitions at ca. 27000 cm^{-1} (14700 M^{-1} cm^{-1} – **CoL^1**, 24600 M^{-1} cm^{-1} – **Co$_2$L^2**) and 23000 cm^{-1} (14800 M^{-1} cm^{-1} – **CoL^1**, 25800 M^{-1} cm^{-1} – **Co$_2$L^2**) similar to other reported Co salen systems (Figure 4, Table 2).[27, 46] Both neutral complexes have the same overall

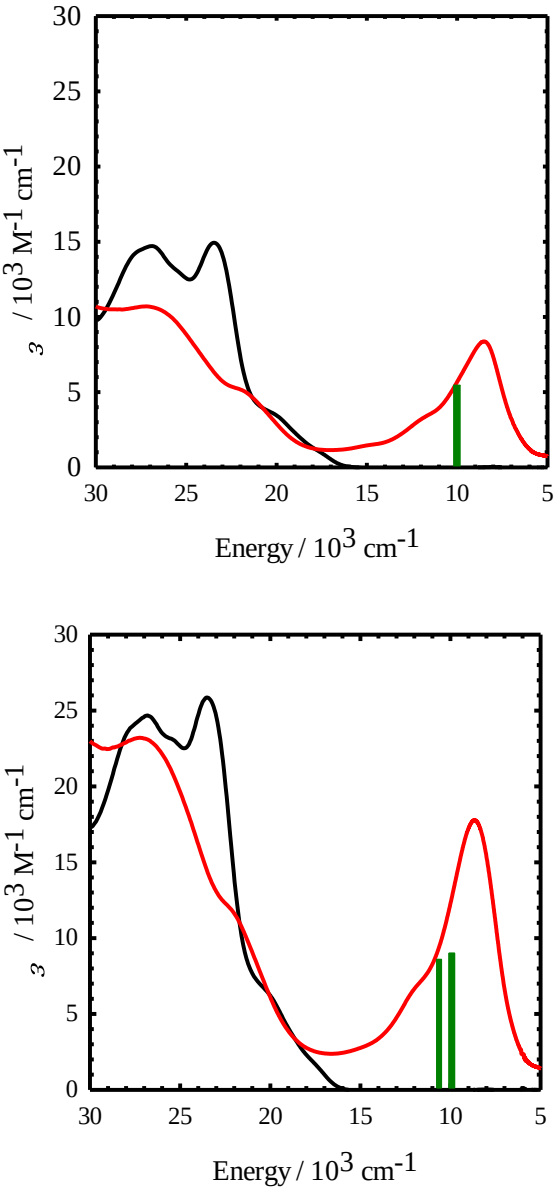

Figure 4. Top: Vis-NIR spectra of **CoL^1** (black line) and **[CoL^1-H$_2$O]$^+$** (red line). Bottom: Vis-NIR spectra of **Co$_2$L^2** (black line) and **[Co$_2$L^2-2H$_2$O]$^{2+}$** (red line). Conditions; CH_2Cl_2, 298 K. DFT predicted transitions are shown as vertical green lines (*vide infra*).

spectral shape, with **Co$_2$L^2** exhibiting double the intensity in comparison to **CoL^1** across all wavelengths, with some minor changes at high energy likely a result of the central phenylene linker. The oxidized complexes display broad high energy

transitions at ca. 27000 cm^{-1} (10700 M^{-1} cm^{-1} – **[CoL^1-H$_2$O]$^+$**, 23200 M^{-1} cm^{-1} – **[Co$_2$L^2-2H$_2$O]$^{2+}$**) and 22000 cm^{-1} (5100 M^{-1} cm^{-1} – **[CoL^1-H$_2$O]$^+$**, 12500 M^{-1} cm^{-1} – **[Co$_2$L^2-2H$_2$O]$^{2+}$**). Low energy transitions for each complex appear at ca. 11 000 cm^{-1} (3600 M^{-1} cm^{-1} – **[CoL^1-H$_2$O]$^+$**, 7700 M^{-1} cm^{-1} – **[Co$_2$L^2-2H$_2$O]$^{2+}$**) and 8500 cm^{-1} (8400 M^{-1} cm^{-1} – **[CoL^1-H$_2$O]$^+$**, 17800 M^{-1} cm^{-1} – **[Co$_2$L^2-2H$_2$O]$^{2+}$**). These transitions are attributed to ligand contributions to the overall electronic structure of the oxidized complexes[25c-e] and the nature of the transitions involved are further analysed by theoretical calculations (*vide infra*). Thomas and co-workers as well as Fujii and co-workers both observed similar low energy bands (~10000 cm^{-1}; ~6000 $M^{-1}cm^{-1}$) in their studies of oxidized monomeric cobalt salen complexes.[27] Both groups studied the same salen ligand, the differences in the two complexes being the axially bound ligand (H_2O *vs* triflate) as well as the presence of an SbF_6 counter ion in the work of Thomas *et al*. The low energy band observed in this work for **[CoL^1-H$_2$O]$^+$** appears at lower energy (8500 cm^{-1}) and is also more absorbing (8400 M^{-1} cm^{-1}), a result attributable to slight differences in ligand electronics. Furthermore, we investigated the temperature dependence of the low energy band (Figure S7) at 298K and 190K. No differences in the band were observed in this temperature range, suggesting that the complex is best described as a single electronic isomer in the temperature range studied.

Table 2. Spectroscopic properties of the Co complexes in CH_2Cl_2 solution

Complex[a]	λ_{max} [cm^{-1}] (ε x 10^3 [M^{-1} cm^{-1}])
CoL^1	27700 sh (14.3), 26900 (14.7), 25600 sh (13.1), 23400 (14.8), 20100 sh (3.1)
[CoL^1-H$_2$O]$^+$	27000 (10.7), 21900 (5.1), 11400 (3.6), 8500 (8.4)
Co$_2$L^2	27600 sh (24.0), 26600 (24.6), 25300 sh (23.0), 23300 (25.8), 20100 sh (6.4)
[Co$_2$L^2-2H$_2$O]$^{2+}$	27000 (23.2), 22600 sh (12.5), 11200 sh (7.7), 8600 (17.8)

[a]Conditions: 1 mM complex, CH_2Cl_2, 298 K; sh = shoulder

Similar to the spectra of the neutral complex, the oxidized dimer species **[Co$_2$L^2-2H$_2$O]$^{2+}$** displays a doubling of spectral intensities across all wavelengths, further enforcing the neutral and oxidized bimetallic complexes as two isolated salen units. The low energy band in **[Co$_2$L^2-2H$_2$O]$^{2+}$** (Figure S8) exhibits a ~15% decrease in the overall intensity at 198K, however in the absence of any other characterization data to support a temperature-dependent change in electronic structure, this is likely due to factors such as poor solubility at low temperature.[47]

3.5. Electron Paramagnetic Resonance Spectroscopy. The X-band EPR spectra of neutral and oxidized complexes is presented in Figure S9. **CoL^1** displays an EPR spectrum which is consistent with a low spin Co(II) (S = ½) ground state. Based on reports by our group[48] and others,[49] **CoL^1** exhibits a |yz, $^2A_2$⟩ ground state in frozen CH_2Cl_2 with hyperfine splitting originating from the I = $^7/_2$ Co nucleus. The dimeric complex, **Co$_2$L^2**, exhibits a similar spectral shape which can be attributed to two 4-coordinate Co(II) (S =½) metal centres, both with |yz, $^2A_2$⟩ ground states in frozen CH_2Cl_2. An eight-line pattern is clearly resolvable at low field (g ~ 3.35). Further evidence for a lack of metal-metal interaction between the two cobalt centres in **Co$_2$L^2** can be found from the EPR spin integration ratio of **Co$_2$L^2** to **CoL^1** of ~2.2; indicating little coupling between metal centers. The above EPR analysis is further corroborated by theoretical calculations and solid-state magnetic studies (*vide infra*).

The X-band EPR spectra of oxidized analogues **[CoL^1-H$_2$O]$^+$** and **[Co$_2$L^2-2H$_2$O]$^{2+}$** are also displayed in Figure S9. Unfortunately the expected transitions associated with the oxidized complexes are likely outside of the energy range of X-band EPR. This data is in agreement with previous results,[27] although Thomas *et. al.* do observe a strong ligand radical signal centered around g~2 in the Q-band EPR spectrum.

3.6. Solid State Magnetics. The magnetic susceptibility (χ_M) *vs*. temperature (T) data for **Co$_2$L^2**, **[CoL^1-H$_2$O]$^+$** and **[Co$_2$L^2-2H$_2$O]$^{2+}$** were obtained between 1.8 and 300 K under a dc applied field of 10 000 Oe and the $\chi_M T$ *vs* T plots are presented in Figures 5 and 6 respectively. For **Co$_2$L^2**, at room temperature, the $\chi_M T$ *vs* T product (Figure 5) of 1.06 cm^3 K mol^{-1} corresponds closely to the expected value of 1.08(1) cm^3 K mol^{-1} (g ~ 2.40; S = ½; C = 0.54 cm^3 K mol^{-1}) for two non-interacting square planar Co(II) centers.

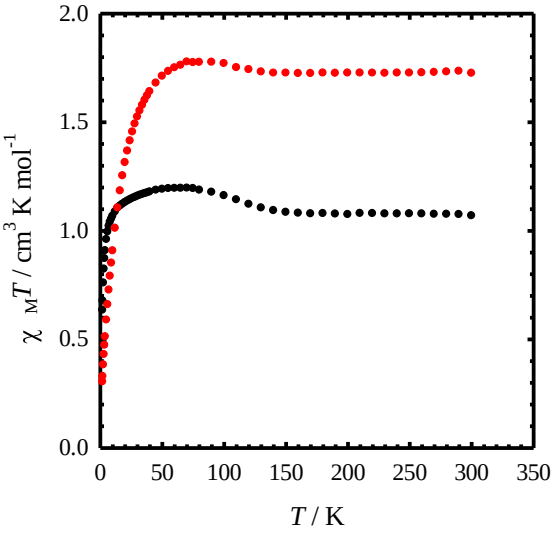

Figure 5. $\chi_M T$ *vs* T data for **Co$_2$L^2** (black spheres) and **[Co$_2$L^2-2H$_2$O]$^{2+}$** (red spheres) at 10 000 Oe between 1.8 and 300 K.

As the temperature is decreased, the $\chi_M T$ *vs* T product increases slowly to a maximum of 1.20(1) cm^3 K mol^{-1} at 70 K followed by a sharp decrease down to 0.63(1) cm^3 K mol^{-1} at 1.8 K. The change in $\chi_M T$ *vs* T with temperature suggests the presence of a combination of both weak ferromagnetic and antiferromagnetic interactions in the system. The $\chi_M T$ *vs* T data above 40 K was fitted (see Figure S10), however, the full

temperature range data could not be fitted using a standard Ising-Heisenberg model. The sharp decrease at low temperature can be caused by the presence of magnetic anisotropy and/or thermal depopulation of the low lying excited states. The field dependence of the magnetization was also measured for **Co_2L^2** at 1.8, 3, 5 and 8 K and is shown in Figure S11. At 1.8 K, the magnetization increases up to a maximum of 2.27(1) μ_β and does not saturate which suggests the presence of anisotropy in the system.

For **$[CoL^1\text{-}H_2O]^+$**, the $\chi_M T$ *vs* *T* product (Figure 6) at room temperature is 1.08 cm^3 K mol^{-1} which is slightly higher than the expected product of 0.915 cm^3 K mol^{-1} for a *S* = 1 system. Fits to the data were compared for both a d^7 Co(II) ligand radical electronic structure, and a high spin Co(III) complex. For the d^7 Co(II) system this includes one non-interacting *S* = ½ Co(II) unit (g ~ 2.40; C = 0.54 cm^3 K mol^{-1}) and one *S* = ½ ligand radical with a fixed g = 2.00 (C = 0.375 cm^3 K mol^{-1}) at 298 K. As the temperature decreases, the $\chi_M T$ *vs* *T* product slowly decreases down to a minimum of 0.12(1) cm^3 K mol^{-1} at 1.8 K suggesting the presence of antiferromagnetic interactions in the system. The field dependence of the magnetization data (Figure S12) was measured between 0 and 7 T and increases steadily to a maximum of 0.68 μ_β at 7 T which indicates the presence of high anisotropy. The $\chi_M T$ *vs* *T* data was well fitted to the Bleaney-Bowers equation[50] (Eqn 1 and Eqn 2) resulting in the fitting parameters of g = 2.41(1) and *J* = -5.2(1) cm^{-1} (Figure 6, red line). This result suggests a weak antiferromagnetic interaction between the Co(II) center and the ligand radical for **$[CoL^1\text{-}H_2O]^+$**. However, the $\chi_M T$ *vs* *T* data could also be fit to a *S* = 1 system of a high spin Co(III) centre ([D] = 32.3 cm^{-1}; g = 2.079; χ_{TIP} < 1 x 10^{-9} emu; blue line),[51] showing that both electronic descriptions satisfy the solid state magnetism data. This analysis is in agreement with a similar oxidized Co salen complex (triflate axial ligand) recently reported by Kurhashi and Fujii.[27b]

$$H = -2J\left[\hat{S}_1 \hat{S}_2\right] \quad (1)$$

$$\chi_M T = \frac{2N\beta^2 g^2}{k} \frac{[1]}{\left[3+\exp\left(-\frac{2J}{kT}\right)\right]} \quad (2)$$

Interestingly, in work reported by Thomas *et al.*, solid state magnetic data (1.47 cm^3 K mol^{-1}) supports a high spin Co(II) center strongly antiferromagnetically coupled to a phenoxyl radical for an oxidized Co salen complex with an axial water ligand.[27a] These results suggest that the electronic structure of oxidized co salen complexes is sensitive to packing in the solid state, in addition to the donating ability of both the salen and axial ligand.

For **$[Co_2L^2\text{-}2H_2O]^{2+}$**, the $\chi_M T$ *vs* *T* product (Figure 5) at room temperature is 1.72(1) cm^3 K mol^{-1} which is close to the expected value of 1.83 cm^3 K mol^{-1} for two non-interacting *S* = ½ Co(II) metal centres (g ~ 2.40; C = 0.54 cm^3 K mol^{-1}) and two non-interacting *S* = ½ ligand radials (g ~ 2.00; C = 0.375 cm^3 K mol^{-1}). Similarly to **Co_2L^2**, as the temperature decreases, the $\chi_M T$ *vs* *T* product increases up to a maximum of 1.77(1) cm^3 K mol^{-1} at 90 K and then sharply decreases down to a value of 0.29(1) cm^3 K mol^{-1} at 1.8 K. This suggests the presence of at least one ferromagnetic and one antiferromagnetic interaction in the system, similarly to **Co_2L^2**. The data however could not be fitted to a standard Ising-Heisenberg model, most likely due to the presence of high anisotropy in the system as supported by the absence of saturation in the M *vs* H data (Figure S13), which increases steadily up to the maximum value of 1.23 μ_β at 7T.

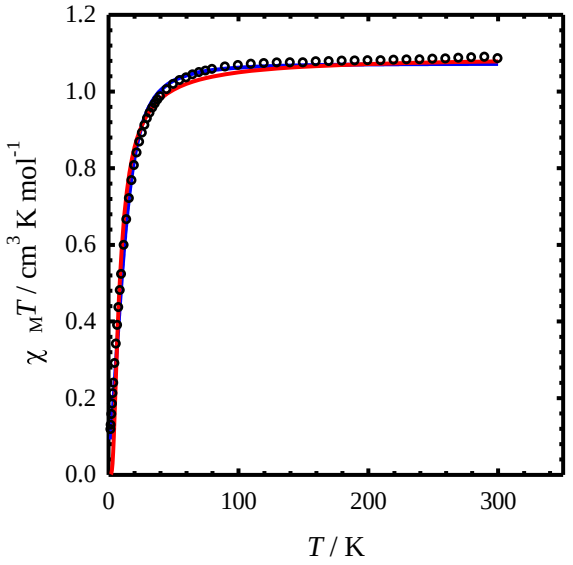

Figure 6. $\chi_M T$ *vs* *T* data for **$[CoL^1\text{-}H_2O]^+$** at 10 000 Oe between 1.8 and 300 K (hollow spheres). The solid red line represents the fit to the data for a *S* = ½ Co(II) unit (g ~ 2.40, C = 0.54 cm^3 K mol^{-1}) antiferromagnetically-coupled (*J* = -5.2(1) cm^{-1}) to a *S* = ½ ligand radical with a fixed g = 2.00 (C = 0.375 cm^3 K mol^{-1}). The solid blue line represents the fit to a *S* = 1 Co(III) complex ([D] = 32.3 cm^{-1}, g = 2.079, χ_{TIP} < 1 x 10^{-9} emu).

3.7. Theoretical Analysis. *3.6.1. Neutral CoL^1 and Co_2L^2.* Density functional theory (DFT) calculations on both neutral and oxidized complexes provided further insight into their geometric and electronic structures. We first compared the optimized geometry of neutral **CoL^1** and **Co_2L^2** with the experimental metrical data. The calculations reproduce the coordination sphere bond lengths to within 0.02 Å (Table 3). In addition, the calculations correctly predict the slight asymmetry in the coordination sphere due to the asymmetric salen ligands. The VT ^{1}H NMR spectroscopy results suggest that **Co_2L^2** is able to freely rotate about the phenylene linker and as such we calculated the energy of the *cis* and *trans* conformers. The *trans* orientation is predicted to be 0.42 kcal mol^{-1} lower in energy than the *cis* orientation, demonstrating the nearly isoenergetic nature of the two conformers; however, due to the solid state structure of **Co_2L^2** exhibiting the cis conformation, we carried out all further calculations on this conformer. The electronic structure of the neutral complexes,

Table 3. Experimental[a] and calculated (in parentheses)[b] coordination sphere metrical parameters for the complexes in [Å].

	CoL^1	$[CoL^1\text{-}H_2O]^+$ (S = 1)	$[CoL^1\text{-}H_2O]^+$ (S = 0)	Co_2L^2 (S = 1)	Co_2L^2 (S = 0)
Co1-O1	1.875 (1.853)	1.868 (1.848)	1.868 (1.873)	1.869 (1.861)	1.869 (1.861)
Co1-O2	1.835 (1.832)	1.846 (1.837)	1.846 (1.852)	1.827 (1.840)	1.827 (1.840)
Co1-N1	1.860 (1.863)	1.891 (1.884)	1.891 (1.880)	1.848 (1.870)	1.848 (1.870)
Co1-N2	1.872 (1.866)	1.892 (1.883)	1.892 (1.885)	1.857 (1.875)	1.857 (1.875)
Co1-O3[c]		2.124 (2.186)	2.124 (2.235)		
Co2-O3[d]				1.861 (1.854)	1.861 (1.853)
Co2-O4				1.838 (1.832)	1.838 (1.832)
Co2-N3				1.856 (1.862)	1.856 (1.862)
Co2-N4				1.888 (1.867)	1.888 (1.866)
Co1---Co2				10.03 (9.382)	10.03 (9.383)

[a]Average of two values for experimental data. [b]See the Experimental Section for calculation details. [c]O3 corresponds to axial water, see Figure 3. [d]O3 corresponds to phenol oxygen, see Figure 1.

and in particular the singularly occupied molecular orbitals (SOMOs) were further investigated, and the DFT calculations accurately predict the metal based character (d_{zy}, d_{z2}) of the SOMOs for both complexes, highlighting the |yz, $^2A_2$> ground states as determined by EPR spectroscopy (Figure S14). Further evidence for a lack of electronic communication between Co centres in $\mathbf{Co_2L^2}$ is exemplified by the isoenergetic nature of the triplet and broken symmetry electronic solutions (ΔE = 0.005 kcal mol^{-1}).

3.6.2. $[CoL^1\text{-}H_2O]^+$ and $[Co_2L^2\text{-}2H_2O]^{2+}$. Upon oxidation, a number of potential electronic structures are possible and we sought to determine a computational model that accurately predicted experimental results for $\mathbf{CoL^1}$ in order to apply to the more computationally taxing $\mathbf{Co_2L^2}$. Possible electronic structure descriptions of one electron oxidized $\mathbf{CoL^1}$ include diamagnetic Co(III)-salen (Co^{3+}-L), high spin Co(III)-salen (↑↑Co^{3+}-L), low-spin Co(II) coupled anti or ferromagnetically to a salen ligand radical, (↑Co^{2+}-↓L•) or (↑Co^{2+}-↑L•) and the high-spin states of the previous descriptions, (↑↑↑Co^{2+}-↓L•) or (↑↑↑Co^{2+}-↑L•). The Co(III) singlet electronic structure is much higher in relative energy in comparison to all other calculated electronic structures, matching the experimental evidence supporting an alternative electronic structure (Table 4). Interestingly, the high spin Co(III)-salen (↑↑Co^{3+}-L), low spin Co(II) ligand radical (↑Co^{2+}-↑L•), and high spin (↑↑↑Co^{2+}-↓L•) initial guesses converge to the same electronic solution, referred to as the triplet solution for the remainder of the article. This solution is predicted to be lowest in energy (Table 4) and supports strong metal and ligand frontier orbital mixing in the oxidized complex. Geometrically, the coordination sphere is best replicated by the triplet and broken symmetry singlet (↑Co^{2+}-↓L•) solutions with the bond lengths of the four coordinate salen atoms reproduced within 0.02 Å. Table 4 outlines the relative energies between the 5 possible spin states described above. The spin density plots for the two lowest energy electronic structures are presented in Figure 7. As is evident in the spin density plots, binding of an axial water ligand reorders the Co based *d* orbitals such that the ground state orbital is now predominantly d_{z2} in character, in excellent agreement with results obtained in other DFT studies on Co salen complexes.[27a, 48] The majority of unpaired spin is localized to the central metal ion in the triplet (~75%) with the remaining unpaired spin density delocalized across the ligand framework,[27a] highlighting the contributions of the high spin Co(III) and low spin Co(II)L• electronic states. Significantly less spin density is localized at the metal center in ↑Co^{2+}-↓L• (*ca*. 1 electron) with the remaining spin density delocalized across the ligand framework.

Table 4. DFT calculated energy differences of possible spin states for $[CoL^1\text{-}H_2O]^+$.

Solution	Relative Energy / kcal mol^{-1}
Co^{3+}-L (singlet)	+17
Triplet solution	0
Broken symmetry singlet	+2.6
↑↑↑Co^{2+}-↑L•	+6.5

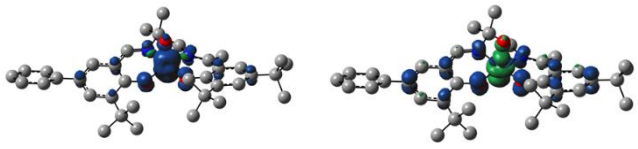

Figure 7. Left: Predicted spin density plot for the triplet solution. Right: Predicted spin density plot for the broken symmetry antiferromagnetically coupled ligand radical solution, ↑Co^{2+}-↓L•.

Time dependent DFT (TD-DFT) accurately predicts the absence of low energy spectral features for $\mathbf{CoL^1}$, while correctly predicting the presence of low energy electronic excitations for $\mathbf{[CoL^1\text{-}H_2O]^+}$. One band of significant intensity

is predicted (10050 cm^{-1}; f = 0.2098), which is slightly blue shifted in comparison to the maximum of the broad low energy transition observed experimentally (Figures 4 and 8). The predicted band is a βHOMO → βLUMO transition and AOMix[43] decomposition of relevant MOs into constituent components indicates that the predicted transition is predominantly a ligand to metal charge transfer band (LMCT) with a shift in electron density from the salen ligand to the metal d_{yz} orbital. However, even though there is a significant shift in electron density to the Co center, the salen ligand remains the dominant component in both donor and acceptor orbitals. The broken symmetry solution predicts an intense NIR band at low energy (~4200 cm^{-1}, f = 0.1395), however this band is not observed experimentally.

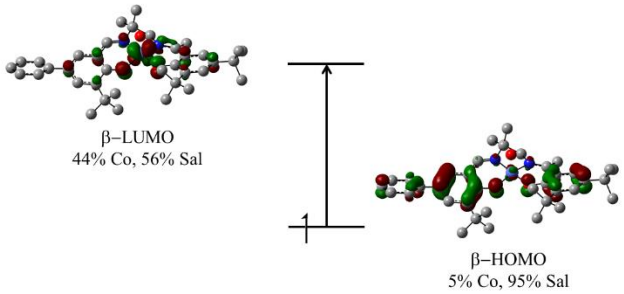

Figure 8. Kohn-Sham molecular orbitals for the triplet solution of **$[CoL^1\text{-}H_2O]^+$** associated with the calculated NIR transition at 10050 cm^{-1} (βHOMO → βLUMO). MO breakdown calculated using AOMix,[43] see the Experimental Section for details.

We then applied the same calculation protocol to **$[Co_2L^2\text{-}2H_2O]^{2+}$,** ignoring high spin Co(II) spin states as they are predicted to be much higher in energy in comparison to the low spin states for **$[CoL^1\text{-}H_2O]^+$**. The two electronic solutions found of lowest energy include an overall quintet electronic structure, incorporating two 'triplet' Co salen units; as well as a BS singlet electronic structure in which ligand radicals and metal based electrons are antiferromagnetically coupled on each salen arm to afford an overall singlet electronic state. The spin density plots of the two electronic structures are shown in Figure 9. The quintet solution is ~8.5 kcal mol^{-1} lower in energy in comparison to the BS singlet electronic structure solution, in line with expected results from the monomer calculations, as well as the experimental magnetic data (Figure S15). Whereas the ligand spin density is equally distributed between both phenolate rings in **$[CoL^1\text{-}H_2O]^+$**, the ligand spin density shifts *slightly* to the outermost phenolate rings in **$[Co_2L^2\text{-}2H_2O]^{2+}$**. Despite this, in both cases the majority (~90 %) of spin density is localized to the central Co ions and N_2O_2 coordination sphere. For **$[Co_2L^2\text{-}2H_2O]^{2+}$**, TD-DFT analysis on the quintet electronic structure solution predicts two low energy transitions that are 353 cm^{-1} apart (Figures 4 and 10). These transitions are βHOMO → βLUMO and βHOMO → βLUMO+1 transitions, respectively and are shown in Figure 10. These transitions, like those of **$[CoL^1\text{-}H_2O]^+$** are both predominantly LMCT in character (as determined by AOMix analysis) in which charge transfers from the phenylene linker to one of the salen units. However, despite these predicted transitions, we do not observe splitting of the low energy band experimentally. We also investigated the TD-DFT transitions of the broken symmetry singlet solution, in which two lower energy bands (~3900 cm^{-1}, f = 0.1298 and ~4600 cm^{-1}, f = 0.1115) are predicted. These bands however, are not observed experimentally and our characterization data together with the data for **$[CoL^1\text{-}H_2O]^+$** strongly supports a quintet electronic structure for **$[Co_2L^2\text{-}2H_2O]^{2+}$**.

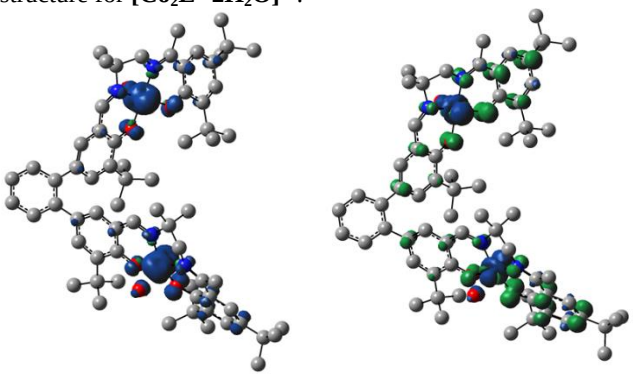

Figure 9. Left: Predicted spin density plot for the quintet (bis triplet) spin state. Right: Predicted spin density plot for the bis broken symmetry singlet solution.

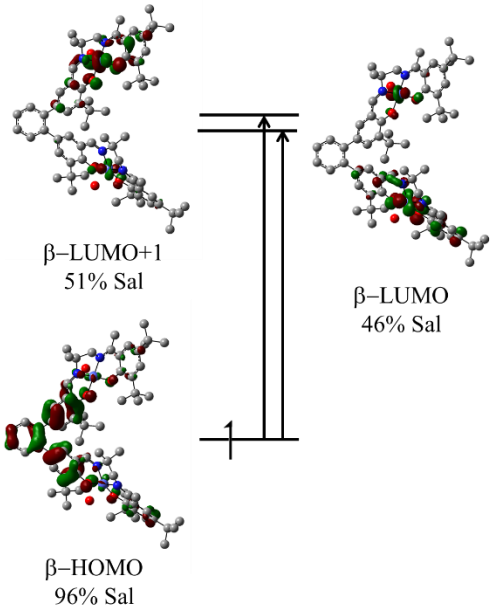

Figure 10. Kohn-Sham molecular orbitals for the triplet solution of **$[Co_2L^2\text{-}2H_2O]^{2+}$** associated with the calculated NIR transitions at 10403 cm^{-1} (βHOMO → βLUMO) and 10757 cm^{-1} (βHOMO → βLUMO+1). MO breakdown calculated using AOMix, see the Experimental Section for details.

3.8 Double Oxidation of CoL^1. Investigation of the CV spectrum of **$[CoL^1\text{-}H_2O]^+$** reveals splitting of the higher

potential, two-electron redox process into independent one electron processes separated by ~200 mV at 233 K (Figure S16). This splitting allowed us to investigate the oxidation of **CoL^1** to the bis-oxidized form using the aminium radical chemical oxidant $[N(C_6H_3Br_2)_3]^{+\bullet}[SbF_6]^-$ (E_{ox} = 1.1 V vs F_c^+/F_c in CH_2Cl_2). Sequential addition of oxidant under an inert atmosphere at 198 K resulted in clean conversion to the doubly oxidized species with isosbestic points at 12000 cm^{-1}, 20000 cm^{-1} and 23000 cm^{-1} (Figure 11). The doubly oxidized species exhibits a broad shoulder at ~8700 cm^{-1} (ε = 1700 M^{-1} cm^{-1}) and a more intense band at 15000 cm^{-1} (ε = 6800 M^{-1} cm^{-1}), similar to the electronic spectra observed in other reports on Co(III)-phenoxyl radical species.[52] The overall spectral shape is in good agreement with that observed by Thomas *et. al.* for an electrochemically generated Co salen doubly oxidized complex.[27a] Furthermore, the EPR spectra for the doubly oxidized species consists of an S = ½ signal centered at g = 2.00 (Figure 12). A g value that is slightly lower than the free electron g value (g_e = 2.002) is common in Co(III) complexes bearing a phenoxyl radical, and thus lends support to this electronic structure description for the doubly oxidized complex herein.[52a, 53] This is further emphasized by the appearance of a ^{57}Co hyperfine interaction, observed as shoulders on the S = ½ peak although not fully resolved due to broadening of the experimental spectrum. The hyperfine coupling is on the order of ~1.2 mT which is in agreement with hyperfine coupling constants observed in the EPR spectra of other Co(III)-phenoxyl radical complexes.[52a, 52c]

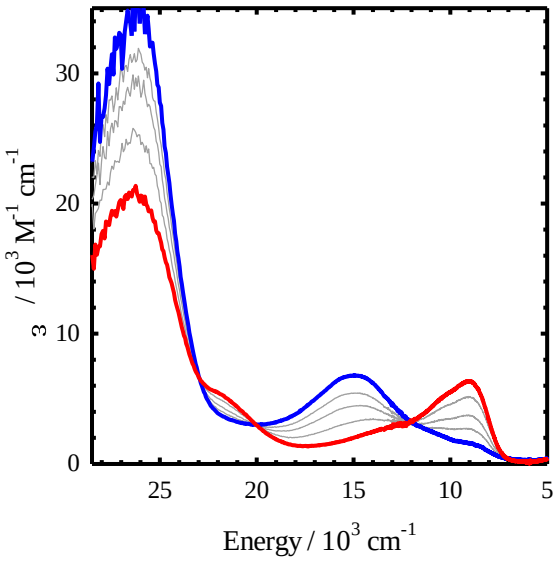

Figure 11. Oxidation titration of **[CoL^1-H$_2$O]$^+$** (red line) to the doubly oxidized species (blue line) with the chemical oxidant $[N(C_6H_3Br_2)_3]^{+\bullet}[SbF_6]^-$. Intermediate gray lines are measured upon sequential addition of oxidant during the titration. Conditions; CH_2Cl_2, 198 K.

The experimental evidence for an electronic structure consisting of a Co(III) metal centre bound to a phenoxyl radical is further corroborated by DFT analysis on the doubly oxidized species with two axially bound water molecules, **[CoL^1-2H$_2$O]$^{2+}$**. The spin-density plot of DFT optimized **[CoL^1-2H$_2$O]$^{2+}$** is depicted in Figure S18, 98% of which is localized to the phenyl substituted side of the salen ligand. This result further emphasizes that double oxidation of **CoL^1** results in a species with a Co(III)-phenoxyl radical electronic structure.

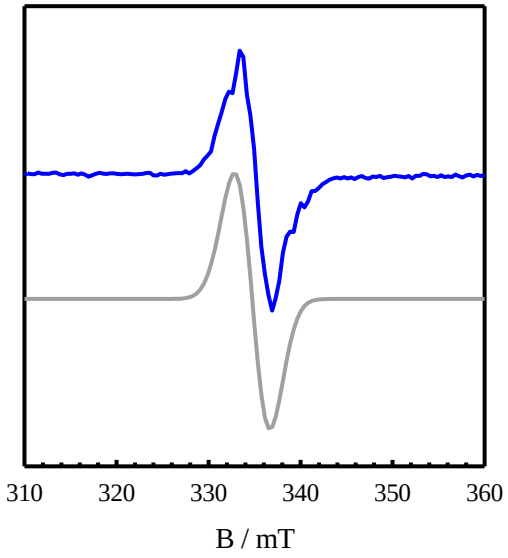

Figure 12. X-band EPR spectra of doubly oxidized **CoL^1** in frozen CH_2Cl_2 with g = 2.00 (blue line). Simulation (grey line). Conditions: frequency = 9.378; power = 2.0 mW; modulation frequency = 100 kHz; modulation amplitude = 0.6 mT; T = 110 K.

4. Discussion and Summary

Neutral complexes **CoL^1** and **Co$_2$L^2** were prepared and characterization of both complexes is consistent with the formation of low spin d^7 Co(II) centers bound to di-anionic, closed shell salen ligands on the basis of EPR, NMR and X-ray diffraction techniques. The central Co ion in **CoL^1** exists in a slightly distorted square planar environment in the solid state. This distortion is also present in the bimetallic complex **Co$_2$L^2**. Of particular interest is the lack of spin-spin coupling between the two metal-localized unpaired spins in **Co$_2$L^2**. Characterization techniques such as cyclic voltammetry, Vis-NIR and EPR all display a doubling of spectral intensities relative to **CoL^1**, consistent with a description of **Co$_2$L^2** having two independent metal-salen units. Although solid state magnetic SQUID data does suggest limited coupling at low temperature, the high magnetic anisotropy in the system prevents more detailed analysis. These results agree well with expected findings based on the large intramolecular metal-

metal separation distance of *ca.* 10 Å between the two Co centers in the complex.

The geometric and electronic structure of oxidized analogues were studied, using **[CoL^1-H$_2$O]$^+$** to inform the characterization of **[Co$_2$L^2-2H$_2$O]$^{2+}$**. Upon oxidation **CoL^1** gains an apically bound water molecule, in similar fashion to the structure reported by Thomas *et. al.*[27a]. Unfortunately, we were unable to obtain X-ray quality crystals of **[Co$_2$L^2-2H$_2$O]$^{2+}$** likely due to the many possible conformers the molecule can adopt as well as the presence of two SbF_6 counter ions. However, on the basis of characterization data, **Co$_2$L^2** also gains two water molecules upon oxidation, presumably one apically bound to each of the two Co centers in the complex.

Oxidation of **CoL^1** to **[CoL^1-H$_2$O]$^+$** affords a complex with significant ligand radical character. Solid state magnetism data for **[CoL^1-H$_2$O][SbF$_6$]** can be fit to either a high spin Co(III) complex, or a low spin d^7 Co(II) ligand radical complex with weak antiferromagnetic coupling (J = -5.2(1) cm^{-1}) between the metal and ligand (Figure 6). DFT calculations predict the triplet state to be slightly lower in energy (2.6 kcal mol^{-1}) in comparison to the broken symmetry antiferromagnetic solution. Interestingly, the high spin Co(III) complex (↑↑Co^{3+}-L), low spin Co(II) ligand radical (↑Co^{2+}-↑L•), and high spin (↑↑↑Co^{2+}-↓L•) initial guesses converge to the same triplet electronic solution. Further analysis of the DFT triplet solution show this to be a mixture of both the (↑↑Co^{3+}-L) and (↑Co^{2+}-↑L•) electronic isomers with ca. 75% of the spin density residing on Co. This result is in agreement with paramagnetic NMR data analysis by Kurahashi and Fujii.[27b] Further oxidation of [**CoL^1-H$_2$O]$^+$** affords the doubly oxidized species whose electronic structure is best described as a Co(III) ion bound to a phenoxyl radical. Isosbestic points in the UV-Vis-NIR indicate clean conversion from the singly to doubly oxidized species, while EPR and DFT analysis confirm the presence of a Co(III)-phenoxyl radical electronic structure.

While two separate one electron waves were observed in the CV spectrum of **Ni$_2$L^2**,[16a] a single two-electron process is observed for **Co$_2$L^2** (Figure 2). This result suggests that the locus of oxidation in these geometrically-equivalent systems differs, facilitating weak coupling in the case of **Ni$_2$L^2**. Comparison of the predicted spin densities of the doubly oxidized **Ni$_2$L^2** and **Co$_2$L^2** systems shows that the locus of oxidation is more contracted in the case of the Co derivative with the majority of the spin density centered on the Co and coordinating atoms. In the case of Ni, the spin density is extensively delocalized across the salen moieties, providing a mechanism for increased communication between the two salen units.

Further evidence pointing towards ligand radical character in these systems is evident from the low-energy transitions of moderate intensity in the Vis-NIR spectrum of both **[CoL^1-H$_2$O]$^+$** and **[Co$_2$L^2-2H$_2$O]$^{2+}$**. TD-DFT calculations were used to further investigate the nature of these electronic transitions. For **[CoL^1-H$_2$O]$^+$** the predicted band is predominantly LMCT in character with significant ligand contribution to both donor and acceptor orbitals (Figure 8). The analogous one electron oxidized Ni complex[16a] displays two much more intense low energy bands (9100 cm^{-1} / 9200 M^{-1} cm^{-1} and 4500 cm^{-1} / 27700 M^{-1} cm^{-1}) assigned as ligand-ligand charge transfer (LLCT) bands. The LMCT character of the low energy band for **[CoL^1-H$_2$O]$^+$** results in less overlap between the donor and acceptor orbitals in comparison to the Ni derivative, resulting in lower intensity.[54] The electronic spectrum of **[Co$_2$L^2-2H$_2$O]$^{2+}$** displays a doubling of spectral intensities across all wavelengths in comparison to **[CoL^1-H$_2$O]$^+$**. The low energy envelope of transitions was also investigated by TD-DFT calculations. Two low energy transitions are predicted which fall under the experimentally observed broad band (Figure 4 and 10); and like **[CoL^1-H$_2$O]$^+$**, both transitions are best described as LMCT transitions on the basis of AOMix decomposition analysis. The analogous Ni dimer complex exhibits two intense bands (4890 cm^{-1}/26500 M^{-1} cm^{-1} and 4200 cm^{-1}/21200 M^{-1} cm^{-1}) in place of the single low energy band in the monomeric Ni complex. These bands are equally spaced in comparison to the band observed for the oxidized monomeric complex (~4500 cm^{-1}) and are attributed to exciton coupling in the excited state.[55] The broad low energy band observed in the spectrum of **[Co$_2$L^2-2H$_2$O]$^{2+}$** does not display resolvable splitting; despite two closely spaced transitions predicted by TD-DFT calculations. The interaction between chromophores, leading to exciton coupling is a function of the transition moment dipole of the monomer, and the angle and distance between the transition dipoles in the dimer.[55-56] For an oblique dimer arrangement, as in this case, two bands are expected if certain criteria can be met.[55a, 56-57] T low band intensity, a result of the LMCT character and contracted donor and acceptor orbitals, likely limits exciton coupling in the case of **[Co$_2$L^2-2H$_2$O]$^{2+}$**. Overall, we have shown that the bimetallic Co complex **Co$_2$L^2** can be doubly oxidized to the dication and that each salen unit remains effectively isolated in both neutral and oxidized structures.

Associated Content

Supporting Information

X-ray crystal structure of **CoL^1**, cif files of all structures, ^{1}H NMR data of both complexes, and further magnetic, spectroscopic and computational data. This material is available free of charge via the Internet at http://pubs.acs.org.

Author Information

Corresponding Author

*E-mail: tim_storr@sfu.ca

Notes

The authors declare no competing financial interest.

Acknowledgements

This work is supported by a Natural Sciences and Engineering Research Council (NSERC) Discovery Grant (T.S.). R.M.C. thanks NSERC for a postgraduate fellowship. K.E.P. acknowledges support of a Vanier CGS. Prof. Charles Walsby is thanked for providing access to the EPR facility. Compute Canada and Westgrid are acknowledged for access to computational resources.

References

(1) (a) Pierpont, C. G., *Coord. Chem. Rev.*, **2001**, *216–217*, 99. (b) Chirik, P. J., *Inorg. Chem.*, **2011**, *50*, 9737. (c) Kaim, W., *Eur. J. Inorg. Chem.*, **2012**, *2012*, 343. (d) Luca, O. R.; Crabtree, R. H., *Chem. Soc. Rev.*, **2013**, *42*, 1440. (e) Praneeth, V. K. K.; Ringenberg, M. R.; Ward, T. R., *Angew. Chem. Int. Ed.*, **2012**, *51*, 10228. (f) Chirik, P. J.; Wieghardt, K., *Science*, **2010**, *327*, 794.

(2) (a) Bryliakov, K. P.; Talsi, E. P., *Coord. Chem. Rev.*, **2014**, *276*, 73. (b) Costas, M.; Mehn, M. P.; Jensen, M. P.; Que, L., *Chem. Rev.*, **2004**, *104*, 939. (c) Jazdzewski, B. A.; Tolman, W. B., *Coord. Chem. Rev.*, **2000**, *200–202*, 633. (d) Stone, K. L.; Borovik, A. S., *Curr. Opin. Chem. Biol.*, **2009**, *13*, 114. (e) Groves, J. T., *Nat Chem*, **2014**, *6*, 89.

(3) Whittaker, J. W., *Chem. Rev.*, **2003**, *103*, 2347.

(4) (a) *Cytochrome P450: Structure, Mechanism, and Biochemistry*. 3 ed.; Kluwer Academic/Plenum Publishers: New York, 2005; p 689. (b) Rittle, J.; Green, M. T., *Science*, **2010**, *330*, 933.

(5) (a) Que, L.; Tolman, W. B., *Nature*, **2008**, *455*, 333. (b) Nam, W., *Acc. Chem. Res.*, **2007**, *40*, 465. (c) Swiegers, G. F.; Chen, J.; Wagner, P., Bioinspired Catalysis. In *Bioinspiration and Biomimicry in Chemistry*, John Wiley & Sons, Inc.: 2012; pp 165. (d) Wang, Y.; DuBois, J. L.; Hedman, B.; Hodgson, K. O.; Stack, T. D. P., *Science*, **1998**, *279*, 537. (e) Chen, M. S.; White, M. C., *Science*, **2007**, *318*, 783. (f) Kudrik, E. V.; Afanasiev, P.; Alvarez, L. X.; Dubourdeaux, P.; Clémancey, M.; Latour, J.-M.; Blondin, G.; Bouchu, D.; Albrieux, F.; Nefedov, S. E.; Sorokin, A. B., *Nat Chem*, **2012**, *4*, 1024. (g) Orio, M.; Jarjayes, O.; Kanso, H.; Philouze, C.; Neese, F.; Thomas, F., *Angew. Chem. Int. Ed.*, **2010**, *49*, 4989.

(6) (a) Sproules, S.; Wieghardt, K., *Coord. Chem. Rev.*, **2011**, *255*, 837. (b) Vlcek, A., *Coord. Chem. Rev.*, **2010**, *254*, 1357. (c) Nomura, M.; Cauchy, T.; Fourmigué, M., *Coord. Chem. Rev.*, **2010**, *254*, 1406. (d) Deplano, P.; Pilia, L.; Espa, D.; Mercuri, M. L.; Serpe, A., *Coord. Chem. Rev.*, **2010**, *254*, 1434.

(7) (a) Pierpont, C. G.; Buchanan, R. M., *Coord. Chem. Rev.*, **1981**, *38*, 45. (b) Bhattacharya, S.; Gupta, P.; Basuli, F.; Pierpont, C. G., *Inorg. Chem.*, **2002**, *41*, 5810. (c) Pierpont, C. G., *Coord. Chem. Rev.*, **2001**, *219–221*, 415. (d) Marshall-Roth, T.; Liebscher, S. C.; Rickert, K.; Seewald, N. J.; Oliver, A. G.; Brown, S. N., *Chem. Comm.*, **2012**, *48*, 7826. (e) Das, D.; Sarkar, B.; Kumbhakar, D.; Mondal, T. K.; Mobin, S. M.; Fiedler, J.; Urbanos, F. A.; Jiménez-Aparicio, R.; Kaim, W.; Lahiri, G. K., *Chem. Eur. J.*, **2011**, *17*, 11030.

(8) (a) Sarkar, B.; Schweinfurth, D.; Deibel, N.; Weisser, F., *Coord. Chem. Rev.*, **2015**, *293–294*, 250. (b) Booth, C. H.; Kazhdan, D.; Werkema, E. L.; Walter, M. D.; Lukens, W. W.; Bauer, E. D.; Hu, Y.-J.; Maron, L.; Eisenstein, O.; Head-Gordon, M.; Andersen, R. A., *J. Am. Chem. Soc.*, **2010**, *132*, 17537. (c) Wang, M.; Weyhermüller, T.; England, J.; Wieghardt, K., *Inorg. Chem.*, **2013**, *52*, 12763. (d) Bowman, A. C.; Sproules, S.; Wieghardt, K., *Inorg. Chem.*, **2012**, *51*, 3707. (e) Scarborough, C. C.; Sproules, S.; Weyhermüller, T.; DeBeer, S.; Wieghardt, K., *Inorg. Chem.*, **2011**, *50*, 12446.

(9) (a) Ali, A.; Barman, S. K.; Mukherjee, R., *Inorg. Chem.*, **2015**, *54*, 5182. (b) Hübner, R.; Sarkar, B.; Fiedler, J.; Záliš, S.; Kaim, W., *Eur. J. Inorg. Chem.*, **2012**, *2012*, 3569. (c) Poddel'sky, A. I.; Cherkasov, V. K.; Abakumov, G. A., *Coord. Chem. Rev.*, **2009**, *253*, 291. (d) Thomas, F.; Gellon, G.; Gautier-Luneau, I.; Saint-Aman, E.; Pierre, J.-L., *Angew. Chem. Int. Ed.*, **2002**, *41*, 3047. (e) Michel, F.; Hamman, S.; Thomas, F.; Philouze, C.; Gautier-Luneau, I.; Pierre, J.-L., *Chem. Comm.*, **2006**, 4122. (f) Chiang, L.; Savard, D.; Shimazaki, Y.; Thomas, F.; Storr, T., *Inorg. Chem.*, **2014**, *53*, 5810. (g) Lionetti, D.; Medvecz, A. J.; Ugrinova, V.; Quiroz-Guzman, M.; Noll, B. C.; Brown, S. N., *Inorg. Chem.*, **2010**, *49*, 4687. (h) Kopec, J. A.; Shekar, S.; Brown, S. N., *Inorg. Chem.*, **2012**, *51*, 1239. (i) Ranis, L. G.; Werellapatha, K.; Pietrini, N. J.; Bunker, B. A.; Brown, S. N., *Inorg. Chem.*, **2014**, *53*, 10203. (j) Cipressi, J.; Brown, S. N., *Chem. Comm.*, **2014**, *50*, 7956.

(10) (a) Lyons, C. T.; Stack, T. D. P., *Coord. Chem. Rev.*, **2013**, *257*, 528. (b) Chiang, L.; Kochem, A.; Jarjayes, O.; Dunn, T. J.; Vezin, H.; Sakaguchi, M.; Ogura, T.; Orio, M.; Shimazaki, Y.; Thomas, F.; Storr, T., *Chem. Eur. J.*, **2012**, *18*, 14117. (c) Storr, T.; Verma, P.; Pratt, R. C.; Wasinger, E. C.; Shimazaki, Y.; Stack, T. D. P., *J. Am. Chem. Soc.*, **2008**, *130*, 15448. (d) Storr, T.; Wasinger, E. C.; Pratt, R. C.; Stack, T. D. P., *Angew. Chem. Int. Ed.*, **2007**, *46*, 5198. (e) Rotthaus, O.; Jarjayes, O.; Thomas, F.; Philouze, C.; Del Valle, C. P.; Saint-Aman, E.; Pierre, J. L., *Chem. Eur. J.*, **2006**, *12*, 2293. (f) Rotthaus, O.; Thomas, F.; Jarjayes, O.; Philouze, C.; Saint-Aman, E.; Pierre, J.-L., *Chem. Eur. J.*, **2006**, *12*, 6953. (g) Shimazaki, Y.; Tani, F.; Fukui, K.; Naruta, Y.; Yamauchi, O., *J. Am. Chem. Soc.*, **2003**, *125*, 10512. (h) Shimazaki, Y.; Stack, T. D. P.; Storr, T., *Inorg. Chem.*, **2009**, *48*, 8383. (i) Kurahashi, T.; Fujii, H., *J. Am. Chem. Soc.*, **2011**, *133*, 8307. (j) Shimazaki, Y.; Arai, N.; Dunn, T. J.; Yajima, T.; Tani, F.; Ramogida, C. F.; Storr, T., *Dalton Trans.*, **2011**, *40*, 2469. (k) Chiang, L.; Herasymchuk, K.; Thomas, F.; Storr, T., *Inorg. Chem.*, **2015**, *54*, 5970. (l) Kochem, A.; Jarjayes, O.; Baptiste, B.; Philouze, C.; Vezin, H.; Tsukidate, K.; Tani, F.; Orio, M.; Shimazaki, Y.; Thomas, F., *Chem. Eur. J.*, **2012**, *18*, 1068. (m) Verma, P.; Pratt, R. C.; Storr, T.; Wasinger, E. C.; Stack, T. D. P., *Proc. Natl. Acad. Sci. U. S. A.*, **2011**, *108*, 18600. (n) de Bellefeuille, D.; Askari, M. S.; Lassalle-Kaiser, B.; Journaux, Y.; Aukauloo, A.; Orio, M.; Thomas, F.; Ottenwaelder, X., *Inorg. Chem.*, **2012**, *51*, 12796. (o) Asami, K.; Tsukidate, K.; Iwatsuki, S.; Tani, F.; Karasawa, S.; Chiang, L.; Storr, T.; Thomas, F.; Shimazaki, Y., *Inorg. Chem.*, **2012**, *51*, 12450. (p) Pratt, R. C.; Lyons, C. T.; Wasinger, E. C.; Stack, T. D. P., *J. Am. Chem. Soc.*, **2012**, *134*, 7367. (q) Lecarme, L.; Chiang, L.; Philouze, C.; Jarjayes, O.; Storr, T.; Thomas, F., *Eur. J. Inorg. Chem.*, **2014**, *2014*, 3479.

(11) (a) Whiteoak, C. J.; Salassa, G.; Kleij, A. W., *Chem. Soc. Rev.*, **2012**, *41*, 622. (b) Cozzi, P. G., *Chem. Soc. Rev.*, **2004**, *33*, 410. (c) Baleizão, C.; Garcia, H., *Chem. Rev.*, **2006**, *106*, 3987. (d) Darensbourg, D. J., *Chem. Rev.*, **2007**, *107*, 2388. (e) McGarrigle, E. M.; Gilheany, D. G., *Chem. Rev.*, **2005**, *105*, 1563.

(12) (a) Viciano-Chumillas, M.; Li, D.; Smogunov, A.; Latil, S.; Dappe, Y. J.; Barreteau, C.; Mallah, T.; Silly, F., *Chem. Eur. J.*, **2014**, *20*, 13566. (b) Chakrabarty, R.; Mukherjee, P. S.; Stang, P. J., *Chem. Rev.*, **2011**, *111*, 6810. (c) Yang, X.; Oye, M. M.; Jones, R. A.; Huang, S., *Chem. Comm.*, **2013**, *49*, 9579.

(13) Haak, R. M.; Wezenberg, S. J.; Kleij, A. W., *Chem. Comm.*, **2010**, *46*, 2713.

(14) (a) Konsler, R. G.; Karl, J.; Jacobsen, E. N., *J. Am. Chem. Soc.*, **1998**, *120*, 10780. (b) Mazet, C.; Jacobsen, E. N., *Angew. Chem. Int. Ed.*, **2008**, *47*, 1762. (c) Park, J.; Lang, K.; Abboud, K. A.; Hong, S., *J. Am. Chem. Soc.*, **2008**, *130*, 16484. (d) Mouri, S.; Chen, Z.; Mitsunuma, H.; Furutachi, M.; Matsunaga, S.; Shibasaki, M., *J. Am. Chem. Soc.*, **2010**, *132*, 1255. (e) Handa, S.; Gnanadesikan, V.; Matsunaga, S.; Shibasaki, M., *J. Am. Chem. Soc.*, **2010**, *132*, 4925.

(15) (a) Shibasaki, M.; Kanai, M.; Matsunaga, S.; Kumagai, N., *Acc. Chem. Res.*, **2009**, *42*, 1117. (b) Radlauer, M. R.; Day, M. W.; Agapie, T., *J. Am. Chem. Soc.*, **2012**, *134*, 1478. (c) Radlauer, M. R.; Day, M. W.; Agapie, T., *Organometallics*, **2012**, *31*, 2231. (d) Chen, Q.; Yu, J.; Huang, J., *Organometallics*, **2007**, *26*, 617. (e) Guironnet, D.; Friedberger, T.; Mecking, S., *Dalton Trans.*, **2009**, 8929. (f) Hu, T.; Tang, L.-M.; Li, X.-F.; Li, Y.-S.; Hu, N.-H., *Organometallics*, **2005**, *24*, 2628. (g) Rodriguez, B. A.; Delferro, M.; Marks, T. J., *Organometallics*, **2008**, *27*, 2166. (h) S, S.; Joe, D. J.; Na, S. J.; Park, Y.-W.; Choi, C. H.; Lee, B. Y., *Macromolecules*, **2005**, *38*, 10027. (i) Hirotsu, M.; Ohno, N.; Nakajima, T.; Ueno, K., *Chem. Lett.*, **2005**, *34*, 848. (j) Hirotsu, M.; Ohno, N.; Nakajima, T.; Kushibe, C.; Ueno, K.; Kinoshita, I., *Dalton Trans.*, **2010**, *39*, 139. (k) Hirotsu, M.; Kawamoto, K.; Tanaka, R.; Nagai, Y.; Ueno, K.; Teki, Y.; Kinoshita, I., *Dalton Trans.*, **2013**, *42*, 12220.

(16) (a) Dunn, T. J.; Chiang, L.; Ramogida, C. F.; Hazin, K.; Webb, M. I.; Katz, M. J.; Storr, T., *Chem. Eur. J.*, **2013**, *19*, 9606. (b) Dunn, T. J.; Chiang, L.; Ramogida, C. F.; Webb, M. I.; Savard, D.; Sakaguchi, M.; Ogura, T.; Shimazaki, Y.; Storr, T., *Dalton Trans.*, **2012**, *41*, 7905. (c) Dunn, T. J.; Ramogida, C. F.; Simmonds, C.; Paterson, A.; Wong, E. W. Y.; Chiang, L.; Shimazaki, Y.; Storr, T., *Inorg. Chem.*, **2011**, *50*, 6746. (d) Guo, Z. Q.; Tong, W. L.; Chan, M. C. W., *Chem. Comm.*, **2009**, 6189. (e) Guo, Z. Q.; Yiu, S. M.; Chan, M. C. W., *Chem. Eur. J.*, **2013**, *19*, 8937. (f) Tong, W.-L.; Yiu, S.-M.; Chan, M. C. W., *Inorg. Chem.*, **2013**, *52*, 7114.

(17) (a) Glaser, T.; Heidemeier, M.; Weyhermüller, T.; Hoffmann, R.-D.; Rupp, H.; Müller, P., *Angew. Chem. Int. Ed.*, **2006**, *45*, 6033. (b) Glaser, T.; Heidemeier, M.; Krickemeyer, E.; Bögge, H.; Stammler, A.; Fröhlich, R.; Bill, E.; Schnack, J., *Inorg. Chem.*, **2009**, *48*, 607.

(18) (a) Clarke, R. M.; Storr, T., *Dalton Trans.*, **2014**, *43*, 9380. (b) Hirotsu, M.; Shimizu, Y.; Kuwamura, N.; Tanaka, R.; Kinoshita, I.; Takada, R.; Teki, Y.; Hashimoto, H., *Inorg. Chem.*, **2012**, *51*, 766. (c)

Houjou, H.; Ito, M.; Araki, K., *Inorg. Chem.*, **2011**, *50*, 5298. (d) Yagi, K.; Ito, M.; Houjou, H., *Macromol. Rapid Commun.*, **2012**, *33*, 540.
(19) (a) Rotthaus, O.; Jarjayes, O.; Philouze, C.; Del Valle, C. P.; Thomas, F., *Dalton Trans.*, **2009**, 1792. (b) Glaser, T.; Heidemeier, M.; Strautmann, J. B. H.; Bögge, H.; Stammler, A.; Krickemeyer, E.; Huenerbein, R.; Grimme, S.; Bothe, E.; Bill, E., *Chem. Eur. J.*, **2007**, *13*, 9191. (c) Glaser, T.; Heidemeier, M.; Fröhlich, R.; Hildebrandt, P.; Bothe, E.; Bill, E., *Inorg. Chem.*, **2005**, *44*, 5467. (d) Strautmann, J. B. H.; Freiherr von Richthofen, C.-G.; Heinze-Brückner, G.; DeBeer, S.; Bothe, E.; Bill, E.; Weyhermüller, T.; Stammler, A.; Bögge, H.; Glaser, T., *Inorg. Chem.*, **2011**, *50*, 155. (e) Rotthaus, O.; Jarjayes, O.; Thomas, F.; Philouze, C.; Saint-Aman, E.; Pierre, J.-L., *Dalton Trans.*, **2007**, 889.
(20) Collman, J. P.; Wagenknecht, P. S.; Hutchison, J. E., *Angew. Chem. Int. Ed.*, **1994**, *33*, 1537.
(21) Rosenthal, J.; Nocera, D. G., *Acc. Chem. Res.*, **2007**, *40*, 543.
(22) (a) Devoille, A. M. J.; Love, J. B., *Dalton Trans.*, **2012**, *41*, 65. (b) Askarizadeh, E.; Yaghoob, S. B.; Boghaei, D. M.; Slawin, A. M. Z.; Love, J. B., *Chem. Comm.*, **2010**, *46*, 710. (c) Volpe, M.; Hartnett, H.; Leeland, J. W.; Wills, K.; Ogunshun, M.; Duncombe, B. J.; Wilson, C.; Blake, A. J.; McMaster, J.; Love, J. B., *Inorg. Chem.*, **2009**, *48*, 5195. (d) Givaja, G.; Volpe, M.; Edwards, M. A.; Blake, A. J.; Wilson, C.; Schröder, M.; Love, J. B., *Angew. Chem. Int. Ed.*, **2007**, *46*, 584.
(23) Benisvy, L.; Bill, E.; Blake, A. J.; Collison, D.; Davies, E. S.; Garner, C. D.; Guindy, C. I.; McInnes, E. J. L.; McArdle, G.; McMaster, J.; Wilson, C.; Wolowska, J., *Dalton Trans.*, **2004**, 3647.
(24) (a) Poddel'sky, A. I.; Cherkasov, V. K.; Fukin, G. K.; Bubnov, M. P.; Abakumova, L. G.; Abakumov, G. A., *Inorg. Chim. Acta*, **2004**, *357*, 3632. (b) Herebian, D.; Ghosh, P.; Chun, H.; Bothe, E.; Weyhermüller, T.; Wieghardt, K., *Eur. J. Inorg. Chem.*, **2002**, *2002*, 1957. (c) Bill, E.; Bothe, E.; Chaudhuri, P.; Chlopek, K.; Herebian, D.; Kokatam, S.; Ray, K.; Weyhermüller, T.; Neese, F.; Wieghardt, K., *Chem. Eur. J.*, **2005**, *11*, 204. (d) Smith, A. L.; Clapp, L. A.; Hardcastle, K. I.; Soper, J. D., *Polyhedron*, **2010**, *29*, 164. (e) Smith, A. L.; Hardcastle, K. I.; Soper, J. D., *J. Am. Chem. Soc.*, **2010**, *132*, 14358. (f) Dzik, W. I.; van der Vlugt, J. I.; Reek, J. N. H.; de Bruin, B., *Angew. Chem. Int. Ed.*, **2011**, *50*, 3356.
(25) (a) van der Meer, M.; Rechkemmer, Y.; Peremykin, I.; Hohloch, S.; van Slageren, J.; Sarkar, B., *Chem. Comm.*, **2014**, *50*, 11104. (b) Khusniyarov, M. M.; Harms, K.; Burghaus, O.; Sundermeyer, J.; Sarkar, B.; Kaim, W.; van Slageren, J.; Duboc, C.; Fiedler, J., *Dalton Trans.*, **2008**, 1355. (c) Ray, K.; Begum, A.; Weyhermüller, T.; Piligkos, S.; van Slageren, J.; Neese, F.; Wieghardt, K., *J. Am. Chem. Soc.*, **2005**, *127*, 4403. (d) Ray, K.; Petrenko, T.; Wieghardt, K.; Neese, F., *Dalton Trans.*, **2007**, 1552. (e) Sproules, S.; Kapre, R. R.; Roy, N.; Weyhermüller, T.; Wieghardt, K., *Inorg. Chim. Acta*, **2010**, *363*, 2702.
(26) Jacobsen, E. N., *Acc. Chem. Res.*, **2000**, *33*, 421.
(27) (a) Kochem, A.; Kanso, H.; Baptiste, B.; Arora, H.; Philouze, C.; Jarjayes, O.; Vezin, H.; Luneau, D.; Orio, M.; Thomas, F., *Inorg. Chem.*, **2012**, *51*, 10557. (b) Kurahashi, T.; Fujii, H., *Inorg. Chem.*, **2013**, *52*, 3908.
(28) (a) Kieboom, A. P. G., *Recueil des Travaux Chimiques des Pays-Bas*, **1988**, *107*, 685. (b) Perrin, D. D.; Armarego, W. L. F., *Purification of Laboratory Chemicals*. 1 ed.; Pergamo Press: New York, 1988.
(29) Murata, Y.; Cheng, F.; Kitagawa, T.; Komatsu, K., *J. Am. Chem. Soc.*, **2004**, *126*, 8874.
(30) (a) Evans, D. F., *J. Chem. Soc.*, **1959**, 2003. (b) Evans, D. F.; Fazakerley, G. V.; Phillips, R. F., *J. Chem. Soc. A*, **1971**, 1931.
(31) Sheldrick, G. M. *SHELXT v2014*, Bruker AXS Inc: Madison, WI.
(32) Hubschle, C. B.; Sheldrick, G. M.; Dittrich, B., *J. Appl. Crystallogr.*, **2011**, *44*, 1281.
(33) Betteridge, P. W.; Carruthers, J. R.; Cooper, R. I.; Prout, K.; Watkin, D. J., *J. Appl. Crystallogr.*, **2003**, *36*, 1487.
(34) van der Sluis, P.; Spek, A. L., *Acta Crystallogr., Sect. A: Found. Crystallogr.*, **1990**, *46*, 194.
(35) Farrugia, L., *J. Appl. Crystallogr.*, **2012**, *45*, 849.
(36) *Persistance of Vision Raytracer (POV-Ray)*, 3.6.2; Persistence of Vision Pty. Ltd.: Victoria, Australia, 2004.
(37) Frisch, M. J.; Trucks, G. W.; Schlegel, H. B.; Scuseria, G. E.; Robb, M. A.; Cheeseman, J. R.; Scalmani, G.; Barone, V.; Mennucci, B.; Petersson, G. A.; Nakatsuji, H.; Caricato, M.; Li, X.; Hratchian, H. P.; Izmaylov, A. F.; Bloino, J.; Zheng, G.; Sonnenberg, J. L.; Hada, M.; Ehara, M.; Toyota, K.; Fukuda, R.; Hasegawa, J.; Ishida, M.; Nakajima, T.; Honda, Y.; Kitao, O.; Nakai, H.; Vreven, T.; Montgomery Jr., J. A.; Peralta, J. E.; Ogliaro, F.; Bearpark, M. J.; Heyd, J.; Brothers, E. N.; Kudin, K. N.; Staroverov, V. N.; Kobayashi, R.; Normand, J.; Raghavachari, K.; Rendell, A. P.; Burant, J. C.; Iyengar, S. S.; Tomasi, J.; Cossi, M.; Rega, N.; Millam, N. J.; Klene, M.; Knox, J. E.; Cross, J. B.; Bakken, V.; Adamo, C.; Jaramillo, J.; Gomperts, R.; Stratmann, R. E.; Yazyev, O.; Austin, A. J.; Cammi, R.; Pomelli, C.; Ochterski, J. W.; Martin, R. L.; Morokuma, K.; Zakrzewski, V. G.; Voth, G. A.; Salvador, P.; Dannenberg, J. J.; Dapprich, S.; Daniels, A. D.; Farkas, Ö.; Foresman, J. B.; Ortiz, J. V.; Cioslowski, J.; Fox, D. J. *Gaussian 09*, Gaussian, Inc.: Wallingford, CT, USA, 2009.
(38) (a) Becke, A. D., *J. Chem. Phys.*, **1993**, *98*, 5648. (b) Stephens, P. J.; Devlin, F. J.; Chabalowski, C. F.; Frisch, M. J., *J. Phys. Chem.*, **1994**, *98*, 11623.
(39) (a) Schäfer, A.; Horn, H.; Ahlrichs, R., *J. Chem. Phys.*, **1992**, *97*, 2571. (b) Schäfer, A.; Huber, C.; Ahlrichs, R., *J. Chem. Phys.*, **1994**, *100*, 5829.
(40) (a) Noodleman, L., *J. Chem. Phys.*, **1981**, *74*, 5737. (b) Noodleman, L.; Case, D. A., Density-Functional Theory of Spin Polarization and Spin Coupling in Iron—Sulfur Clusters. In *Advances in Inorganic Chemistry*, Richard, C., Ed. Academic Press: 1992; Vol. Volume 38, pp 423.
(41) (a) Casida, M. E., In *Recent Advances in Density Functional Methods*, Chong, D. P., Ed. World Scientific: Singapore, 1995; p 155. (b) Stratmann, R. E.; Scuseria, G. E.; Frisch, M. J., *J. Chem. Phys.*, **1998**, *109*, 8218.
(42) (a) Barone, V.; Cossi, M.; Tomasi, J., *J. Chem. Phys.*, **1997**, *107*, 3210. (b) Barone, V.; Cossi, M.; Tomasi, J., *J. Comput. Chem.*, **1998**, *19*, 404. (c) Miertuš, S.; Scrocco, E.; Tomasi, J., *Chem. Phys.*, **1981**, *55*, 117. (d) Tomasi, J.; Mennucci, B.; Cancès, E., *J. Mol. Struct. THEOCHEM*, **1999**, *464*, 211.
(43) (a) Gorelsky, S.; Solomon, E., *Theoretical Chem. Acc.*, **2008**, *119*, 57. (b) Gorelsky, S. I. *AOMix, Program for Molecular Orbital Analysis*, 6.85; 2014. http://www.sg-chem.net/. (c) Gorelsky, S. I.; Lever, A. B. P., *J. Organomet. Chem.*, **2001**, *635*, 187.
(44) Connelly, N. G.; Geiger, W. E., *Chem. Rev.*, **1996**, *96*, 877.
(45) Kemper, S.; Hrobárik, P.; Kaupp, M.; Schlörer, N. E., *J. Am. Chem. Soc.*, **2009**, *131*, 4172.
(46) Huber, A.; Müller, L.; Elias, H.; Klement, R.; Valko, M., *Eur. J. Inorg. Chem.*, **2005**, *2005*, 1459.
(47) The low solubility of $\mathbf{[Co_2L^2\text{-}2H_2O]^{2+}}$ at the concentrations required for observable ^{1}H NMR peak shifting disallowed for an Evan's method NMR experiment.
(48) Chiang, L.; Allan, L. E. N.; Alcantara, J.; Wang, M. C. P.; Storr, T.; Shaver, M. P., *Dalton Trans.*, **2014**, *43*, 4295.
(49) (a) Daul, C.; Schläpfer, C.; von Zelewsky, A., The electronic structure of cobalt(II) complexes with schiff bases and related ligands. In *Inorganic Chemistry and Spectroscopy*, Springer Berlin Heidelberg: 1979; Vol. 36, pp 129. (b) Vinck, E.; Doorslaer, S. V.; Murphy, D. M.; Fallis, I. A., *Chem. Phys. Lett.*, **2008**, *464*, 31.
(50) Bleaney, B.; Bowers, K. D., *Proc. R. Soc. Lond. A.*, **1952**, *214*, 451.
(51) Kahn, O., *Molecular Magnetism*. VCH: New York, 1993; Vol. 1.
(52) (a) Kimura, S.; Bill, E.; Bothe, E.; Weyhermüller, T.; Wieghardt, K., *J. Am. Chem. Soc.*, **2001**, *123*, 6025. (b) Zats, G. M.; Arora, H.; Lavi, R.; Yufit, D.; Benisvy, L., *Dalton Trans.*, **2011**, *40*, 10889. (c) Shimazaki, Y.; Kabe, R.; Huth, S.; Tani, F.; Naruta, Y.; Yamauchi, O., *Inorg. Chem.*, **2007**, *46*, 6083.
(53) (a) Müller, J.; Kikuchi, A.; Bill, E.; Weyhermüller, T.; Hildebrandt, P.; Ould-Moussa, L.; Wieghardt, K., *Inorg. Chim. Acta*, **2000**, *297*, 265. (b) Vinck, E.; Murphy, D. M.; Fallis, I. A.; Strevens, R. R.; Van Doorslaer, S., *Inorg. Chem.*, **2010**, *49*, 2083. (c) Thomas, F.; Arora, H.; Philouze, C.; Jarjayes, O., *Inorg. Chim. Acta*, **2010**, *363*, 3122.
(54) Solomon, E. I.; Gorelsky, S. I.; Dey, A., *J. Comput. Chem.*, **2006**, *27*, 1415.
(55) (a) Kasha, M., *Radiat. Res.*, **1963**, *20*, 55. (b) Kasha, M.; Rawls, H. R.; El-Bayoumi, M. A., *Pure Appl. Chem.*, **1965**, *11*, 371.
(56) Valdes-Aguilera, O.; Neckers, D. C., *Acc. Chem. Res.*, **1989**, *22*, 171.
(57) Yoon, M.-C.; Lee, S.; Tokuji, S.; Yorimitsu, H.; Osuka, A.; Kim, D., *Chem. Sci.*, **2013**, *4*, 1756.

For Table of Contents Only

The neutral and oxidized forms of a bimetallic cobalt(II) complex (**Co_2L^2**), and the monomeric analogue (**CoL^1**), were studied using a number of experimental and theoretical methods. The results demonstrate strong metal and ligand frontier orbital mixing and the presence of both high spin Co(III) and Co(II)L• character in the electronic ground state.